A R C H I V E S O F M E T A L L U R G Y A N D M A T E R I A L S
Volume 53 2008 Issue 1

H.-G. BROKMEIER*,**, S. YI*, J. HOMEYER***

IN-SITU ANALYSIS OF CRYSTALLOGRAPHIC TEXTURES USING HIGH-ENERGY X-RAYS

ANALIZA TEKSTURY KRYSTALOGRAFICZNEJ IN-SITU PRZY UŻYCIU WYSOKOENERGETYCZNYCH PROMIENI X

Hard X-rays with energies higher than 50 keV are characterized by there high penetration power in most materials. In the case of 100 keV to 200 keV X-rays the penetration power is in the same order as for thermal neutrons. Rather big differences between hard X-rays from a storage ring and neutrons are the much higher photon flux of some orders and an excellent brilliance of the photon beam. Both properties allow us a number of new innovative investigations. Texture development belongs to one of the major characteristics of materials processing such as deformation, recovery and recrystallization. In order to describe the influence of the initial texture on the materials anisotropy texture simulations and in- situ texture analyses have to be combined. Loading experiments comparable to standard material tests (stress-strain-curve) were carried out on magnesium-alloys and on aluminium in tension as well as in compression. A loading device with a power up to 20 kN was positioned at the high energy beam line BW5 at HASYLAB-DESY. Due to the high penetration power of 100 keV X-rays, which is in the same order as the penetration power of thermal neutrons, we could use DIN 50125 samples in transmission mode. Sample diameters of 4 mm, 6 mm, 8 mm or 10 mm were cut from rectangular extruded bars with orientations of 0°, 45° and 90° to the extrusion direction. Additionally to standard texture measurements at the initial state and at failure up to five points at the known stress strain curve were chosen for in-situ texture measurements. 100keV X-rays have a short wavelength of 0.1240 Å, so that the Bragg-angles are much lower than for conventional X-rays. An image plate detector covers the whole Debeye-Scherrer cone of some reflections, so that only ω-scans are necessary to get the complete pole figure. Due to the frame of the loading device the ω-rotation is limited to of 145°. First experiments on high temperature applications will complete this contribution on a topic which is by our opinion a growing field in quantitative texture analysis and engineering application.

Keywords: Hard X-rays, in-situ tension, high temperature, magnesium, steel

Przenikliwe promieniowanie rentgenowskie o energii większej niż 50 keV charakteryzuje się wysoką zdolnością penetracji w większości metali. W przypadku energii od 100 keV do 200 keV, zdolność penetracji jest tego samego rzędu jak dla termicznych neutronów. Znaczne różnice pomiędzy przenikliwym promieniowaniem rentgenowskim z pierścienia akumulującego, a neutronami są spowodowane dużo wyższym strumieniem fotonów tego samego rzędu oraz doskonałą luminacją promienia fotonów. Właściwości te pozwalają nam na innowacyjne badania.

Formowanie się tekstury należy do głównych charakterystyk obróbki materiałów takich jak deformacja, zdrowienie i rekrystalizacja. Ażeby opisać wpływ początkowej tekstury na symulacje tekstury anizotropii materiałowej oraz analizy tekstury in-situ połączono eksperymenty. Doświadczenia obciążeniowe były porównywane do standardowych testów materiałowych w rozciąganiu oraz ściskaniu. Urządzenie obciążające z siłą do 20 kN było ustawiane przy linii wysokoenergetycznego promienia BW5 przy HASYLAB-DESY. Z powodu wysokiej zdolności penetracji promieniowanie rentgenowskie 100 keV, które jest tego samego rzędu jak zdolność penetracji termicznych neutronów, używano próbek DIN 50125 w modzie transmisyjnym. Próbki o średnicy 4 mm, 6 mm, 8 mm lub 10 mm były wycinane z prostokątnego wyciskanego pręta z orientacją 0°, 45° i 90° do kierunku wyciskania. Dodatkowo do standardowych pomiarów tekstury w stanie początkowym oraz przy rozrywaniu przy znanej krzywej naprężenia odkształcającego, wybrano pięć punktów do pomiarów tekstury in-situ. Promieniowanie rentgenowskie 100 keV ma długość fali 0.1240 Å, tak że kąty Bragga są znacznie mniejsze niż dla konwencjonalnego promieniowania X. Obraz płyty detektora pokrywa cały stożek Debeya-Scherrera takich samych odbić, tak że tylko ω-skany są konieczne aby uzyskać kompletne figury biegunowe. Z powodu klatki urządzenia obciążającego ω-obrót jest ograniczony do 145°. Pierwsze eksperymenty przy zastosowaniu wysokiej temperatury będą uzupełnione tym rozkładem, który jest naszym zdaniem interesującym obszarem w ilościowej analizie tekstury i zastosowaniu inżynierskim.

* INSTITUTE OF MATERIALS SCIENCE AND ENGINEERING, TECHNICAL UNIVERSITY CLAUSTHAL, GERMANY
** GKSS-RESEARCH CENTRE, MAX-PLANCK-STRASSE 1, GEB. 03, D-21502 GEESTHACHT, GERMANY
*** HASYLAB AT DESY, NOTKE STRASSE, HAMBURG, GERMANY

1. Introduction

The crystallographic texture is one of the major characteristics of polycrystalline materials and widely used in many fields of fundamental and applied research. In all fields such as experimental texture analysis, texture simulations and texture correlations to anisotropic properties improvements were done in recent years. On one hand thermo-mechanical treatments in different combinations (casting, deformation, recovery, annealing, phase transitions) are part of all processing routes, which require in-situ experiments at dedicated states (temperatures, tensile or compressive load) or models to interpret room temperature experiments for high temperature processing (variant selection). In order to verify texture simulations over the whole deformation process, on the other hand, one needs at least experimental data from the initial state and from the final state. Particular in materials with hexagonal crystal structure a continuous change of the activation of different glide systems is expected, so that a continuous documentation of the crystallographic texture is useful.

TABLE 1
Penetration power of different radiations for some metals

instrument	D 5000	BW5	Harwi-II	TEX-2
	Cu-Kα 1.54 Å	s- ray 0.124 Å 100 keV	s-ray 0.062 Å 200 keV	n-ray 1.00 Å
Mg	0.0014 cm	3.4 cm	4.2 cm	6.10 cm
Al	0.0053 cm	1.5 cm	2.7 cm	7.67 cm
Cu	0.0015 cm	0.2 cm	0.5 cm	0.85 cm
Ti	0.0011 cm	0.6 cm	1.3 cm	1.61 cm
Pb	0.0003 cm	0.03 cm	0.04 cm	2.10 cm

The classification of high energy X-rays ranges from about 50 keV up to 450 keV. It is well known that an increasing energy leads to increase of the penetration power. Therefore, standard material testing devices operate from 120 keV to 450 keV due to their application field for non-destructive testing (NDT), such as failure analysis in pipelines, quality control in wheel rims etc. A much higher photon flux combined with a fantastic brilliance was obtained in a storage ring. Compared to material testing tubes with its main application for radiography or tomography, synchrotron radiation was used intensively for diffraction experiments [1–3]. In the case of 100 keV up to 200 keV X-rays the penetration length is in the same order as for thermal neutrons, which are well known in materials science applications (texture and strain analyses) as high penetrating radiation. Table 1 shows a comparison of the penetration length for some common metals of four typical radiations (CuKα – 1.5418 Å, 100 keV synchrotron radiations - 0.124 Å, 200 keV synchrotron radiation – 0.062 Å, thermal neutrons 1.250 Å) [4]. The penetration length is given in cm for a loss of 50% of primary beam intensity. New experimental techniques and new instruments at large scale facilities allow much faster measurements meanwhile, which are absolutely necessary for in-situ experimentation due to creep or recrystallization processes.

Worldwide investigation to improve the application of Mg wrought alloys concentrate in one point on the tension-compression anisotropy of Mg-alloys. Due to the hexagonal crystal structure the existing crystallographic textures influences strongly the activation of glide systems and twinning modes for tension and compression. Not only the tension compression anisotropy is remarkable but also the anisotropic behaviour in rolling and transfer direction. Thus, in-situ investigations were carried on some Mg-alloys to examine strain and texture development during tensile load till failure [5]. Explanations of the texture development were given using visco-plastic self consistent simulations. Another point of interest is the in-situ investigation at high temperatures. A spherical dome furnace was used to perform a first measurement of crystallographic textures in about 1h at the high-energy beamline BW5.

2. Experimental equipment

Hasylab offers two high energy beamline at the storage ring Doris III, whereas BW5 is the older one with some experiences in in-situ experimentation, while the new materials science beamline operated by the GKSS-Research Center was positioned at Harwi-II. Both experiments can operate with a two-dimensional image plate detector (MAR345) having typical exposure times from some seconds. Due to the high energy and the low wavelength one can work with small scattering angles. Consequently a set of complete Debye - Scherrer cones are detected simultaneously as shown in figure 1 for a Mg powder sample. In figure 1a one can see an image plate picture taken in 5 sec. covering a 2-θ range of 6°. The powder pattern includes 15 complete Debye-Scherrer cones, which were integrated and plotted in a sum-diffraction spectrum (Fig. 1b). An excellent agreement between measured and calculated diffraction pattern was obtained. It should be noticed that a glass cylinder of 8 mm in diameter was filled with Mg-powder without any preferred orientation. That means, in the case of a texture measurement up to 15 pole figures can be measured simultaneously.

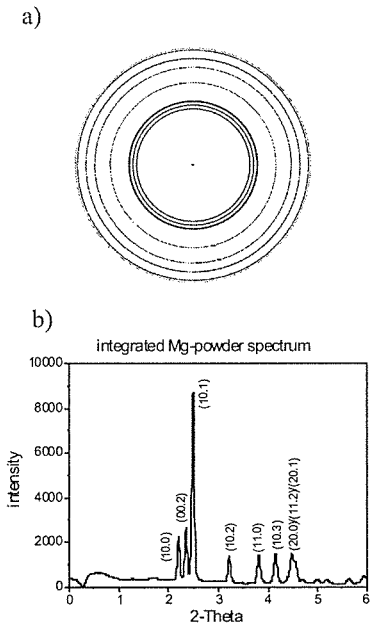

Fig. 1. a) Image plate picture after 5 sec. exposure time of a Mg-powder; b) Sum spectra of the powder pattern in Fig. 1a integrated over the complete Debye-Scherrer rings

The two synchrotron diffractometers are very flexible in changing the energy and the sample to detector distance in a wide range to optimize the experimental conditions. In our case we have used a sample to detector distance of about 100 cm and a wavelength of 0.124 Å. In order to perform in-situ experiments the sample stage was completed by a loading device and/or a furnace. The set up including the loading device mounted on a rotating table and an image plate detector is shown in figure 2.

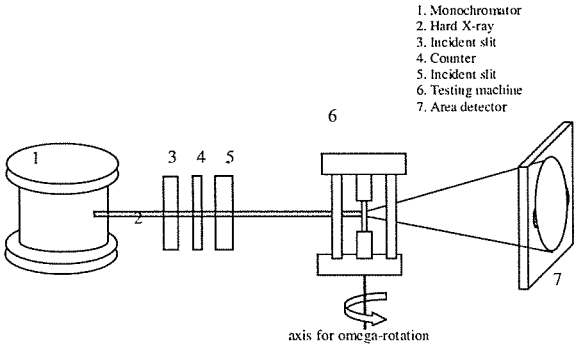

Fig. 2. Principle set up of the synchrotron instrument including a loading device at sample position

The loading device (Fig 3a) has a maximum capacity of 20 kN in tension and in compression [6]. Both types of test samples round with threads of 4mm, 6mm, 8mm and 10mm and flat samples are in use. In parallel to the loading experiment the extension and the loading power were registered. To Harwi-II belongs a huge 100 kN with a high of about 2 m, which was not used in the present study. Three different types of furnaces have been tested. First a mirror furnace of ILL-style with a temperature up to 1600°C was tested [7]. Due to the specification for neutron diffraction at TEX-2, this furnace works but was not optimal. A second furnace shown in figure 3b has a quartz glass dome and a heating system up to 1000°C. The light inside the furnace results from heating a steel sample in the FCC region. A third furnace (see figure 3c) can be combined with the loading device shown in figure 3a. These equipments allow us to investigate lattice thermal expansion, lattice dependent strains, phase transformations, residual and thermal strains, microstructure evolutions and texture evolutions.

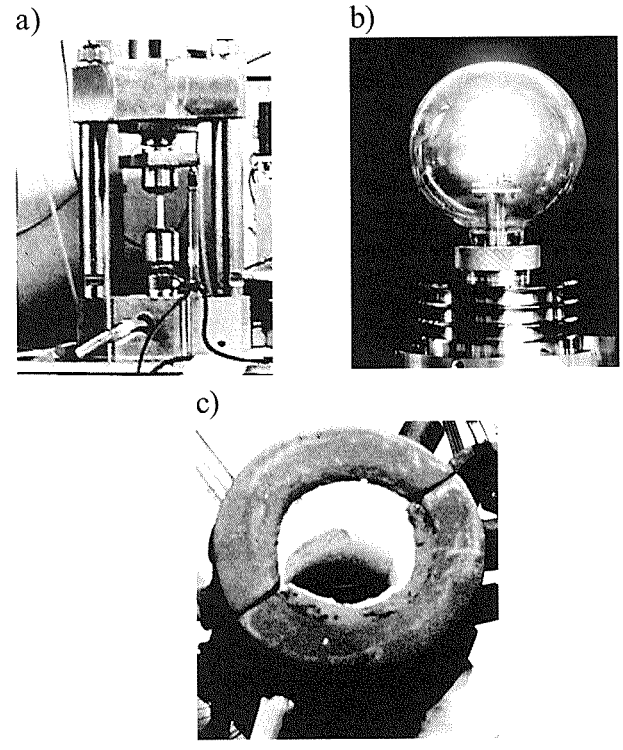

Fig. 3. a) 20kN loading device; b) Quartz class dome furnace; c) Low temperature furnace (450°C) in combination with the loading device

3. In-situ loading

The in-situ loading device can be used from strain as well as for texture measurements. From a rectangular extruded bar a tensile samples were cut in 0°, in 45° and in 90° to the extrusion direction. Figure 4a shows a stress strain curve obtained during the in-situ experiment by an extensometer. The dots express the points at different macro strain levels where the diffraction pattern were taken. Figure 4b shows the sample orientation of the tensile sample with $\sigma_{parallel}$ and $\sigma_{perpendicular}$ directly present in one image plate picture (Fig. 4c). As the figure shows, the diffraction profile from the horizontal (vertical) line on the detector image represents the crystal-

lographic planes perpendicular (parallel) to the loading axis.

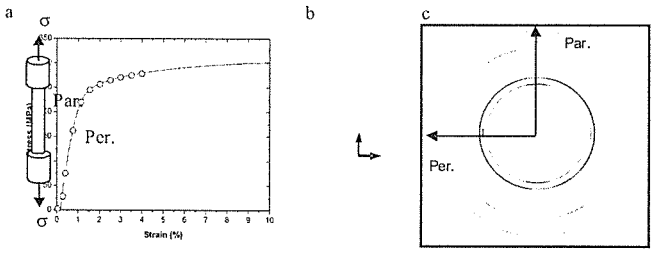

Fig. 4. a) Stress-strain curve with measurement positions for lattice strain measurements; b) Tensile sample with orientation marks; c) Image plate picture of Mg-AZ31 (unstrained)

Figure 5 presents the evolution of internal strains for different {hk.l} during tensile loading. Due to the texture of the present sample three diffraction peaks {10.0}, {10.1} and {11.0} could be evaluated in the loading direction. Because the internal strains parallel to the loading axis are more constrained by external boundary conditions, the internal strains in this direction show more similarity with the stress-strain curve. The internal strains on {10.1} parallel to the loading axis show earlier micro yielding at 0.7% of sample strain. On the other hand the internal strains on {10.0} and {11.0} parallel to the loading axis show later micro yielding at about 1.5% of sample strain. The ratio of the internal strain on {10.0} and {10.1} is 2.4. This means the dislocation gliding on the {10.1} plane, the so called soft-orientation, is relatively easier than on the other planes. The crystallographic planes perpendicular to the loading axis, which are under compression, clearly show also the anisotropic response of internal strains, though the ratio of max. and min. internal strain is smaller than the case of parallel to the loading axis. {00.2} perpendicular to the loading axis shows the hardest behavior, while {10.1} has the softest response of internal strains. It has to be noticed that each image plate picture takes 5 sec. exposure time and about 50 sec. readout time.

The texture measurement needs a number of individual image plate pictures to cover a whole pole figure. A detailed description of this method is given elsewhere [8–11]. That means in-situ pole figure measurements take in the present state between 40 min and 90 min. Due to the construction of the loading device a limitation of the ω-rotation to 140° exists. Consequently, only incomplete pole figures can be measured. In order to overcome this problem the pole figure symmetry can be used or the orientation distribution function (ODF) has to be calculated with incomplete pole figures. As an example the texture evolution of an in-situ tensile test of an Mg AZ31 sample is shown in figure 6 having the tensile axis 90° the extrusion direction.

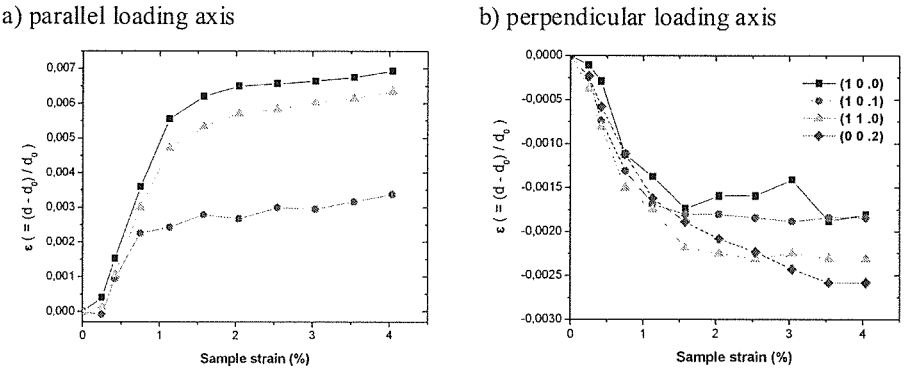

Fig. 5. (hk.l) dependent strains; a – parallel and b – perpendicular to the loading axis

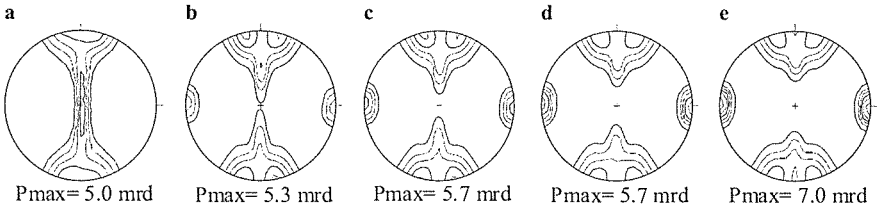

Fig. 6. In-situ texture determination on the 90° sample; (00.2) pole figures a – unloaded sample, b – shortly after the yield points, c – and d – medium positions on the stress strain curve, e – shortly before failure

One can see clearly the development of the crystallographic texture. Both the type of the crystallographic texture and the degree of preferred orientation were changing during tension. As already pointed out above, this texture development correlates with the activation of different glide systems. In addition to the experimental results we simulate the texture development using the viscoplastic self consistent (VPSC) model [12, 13]. For a detailed description of the VPSC – model and a detailed description of the correlation between in-situ texture measurement on Mg-alloys and texture simulation see [14–17]. As an example the development of the different deformation modes of the 90° sample is shown in figure 6. One can see the importance of tensile twins at the beginning of the plastic deformation, which decreases rapidly while basal slip increases. At higher strains a combination of basal, prismatic and pyramidal slip carries the deformation. Twins as well as pyramidal II (c+a) slip are of minor importance. It was demonstrated by textures simulations that the relative activities of the different glide systems depend strongly on the initial texture. The 0° sample as well as the 45° sample (orientation to RD) behaves completely different due to the initial texture.

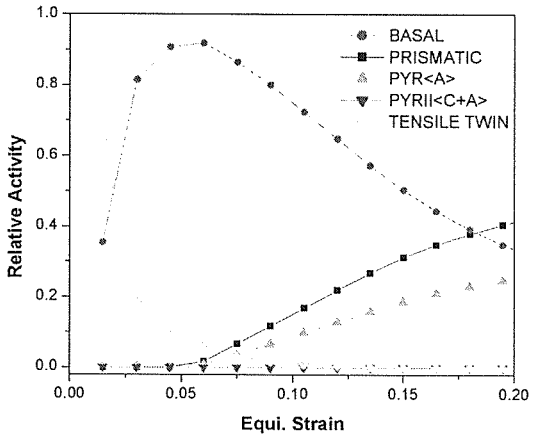

Fig. 7. Development of different deformation modes as a function of the tensile strain

4. In-situ heating

The majority of all processing lines include high temperature treatment such as recovery, recrystallization or phase transition. Thus high temperature phase analysis by X-rays or neutrons is very common. Due to a much longer total counting time high temperature texture analysis is restricted. New instrumentations on high flux beams offer the possibility to measure complete textures in less than 60 min and in the case of high pole figure symmetries in 60 sec. The furnace shown in figure 3b was used to measure textures of shape memory alloys and steel. In the case of the steel experiment a set of only 9 image plate pictures with different ω were taken for the different temperatures with 1 sec. exposure time for each picture. The reduced number of image plate pictures is possible because of the orthorhombic texture symmetry. The program package MAUD (Materials Analysis Using Diffraction) offers on one hand the determination of crystallographic and microstructure data (volume fraction, grain size and strain) using a Rietveld refinement and on the other hand a quantitative texture analyse using a WIMV texture program. Thus we were able to determine the thermal expansion coefficients of α-ferrite, the phase transition (α-ferrite to γ-austenite), the volume fractions in the two phase region and the texture transition. In figure 8 an example is shown for the determination of the volume fractions and the lattice constants in the two phase region α-ferrite/ γ-austenite [18]. Moreover, the texture transition of α-ferrite at room temperature to the high temperature phase γ-austenite was shown. The texture agrees with the Kurdjumov-Sachs orientation relationship for BCC ↔ FCC transformation, $(110)_{BCC}$ //$(111)_{FCC}$.

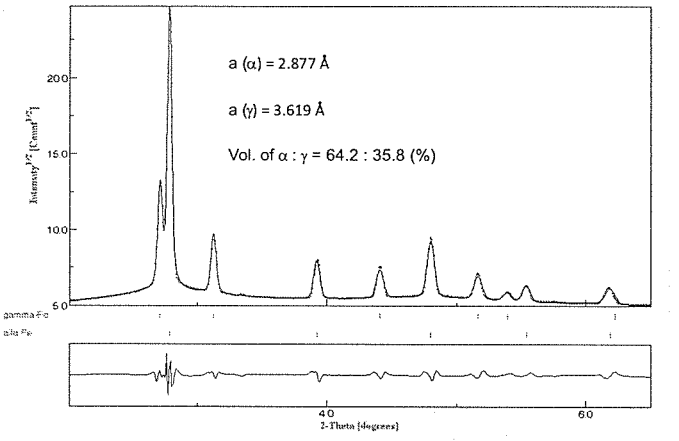

Fig. 8. High temperature investigations on steel; lattice constants and volume fractions of α-ferrite and γ-austenite in the two phase region

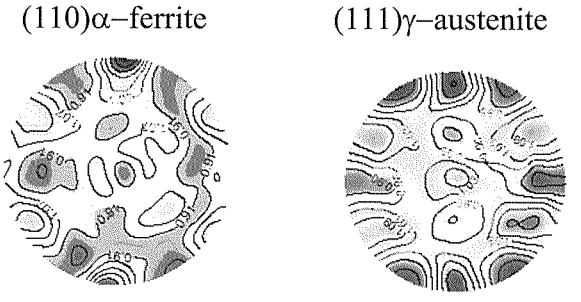

Fig. 9. High temperature investigations on steel; (110) pole figure of α-ferrite at room temperature compared (111) pole figure of γ-austenite at high temperatures

5. Conclusions

First of all it could be recognized that high developed texture instruments at large scale facilities independent which technique (energy dispersive or angular dispersive) and independent which radiation (thermal neutrons or high energy synchrotrons) have an increasing importance on crystallographic texture determination. The present example gives an introduction in some applications carried out at Hasylab/Germany using hard X-rays. Both in-situ loading experiments as well as in-situ heating experiments have a great potential in crystallographic texture analysis. It could be shown, that the texture evolution of an Mg-AZ31 sample during tension correlates with texture simulations and the continuously changing balance between different glide systems plus twinning. For a steel example it is demonstrated that fast measurements allow phase and texture transition, which opens an interesting field of investigations.

Acknowledgements

This work has been funded by the German Ministry of Education and Research (BMBF) under the contract numbers 03BRE8CL and 05KS1MCA/2.

REFERENCES

[1] O.V. Mishin, E.M. Lauridsen, N.C. Krieger Lassen, G. Brückner, T. Tschentcher, B. Bay, D. Juul Jensen, H.F. Poulsen, J. Appl. Crys. **33**, 364 (2000).

[2] L. Wcislak, H. Klein, H.J. Bunge, U. Garbe, T. Tschentscher, J. Schneider, J. Appl. Cryst. **35**, 82 (2002).

[3] H.-R. Wenk, S. Grigull, J. Appl. Cryst. **36**, 1040 (2003).

[4] H.-G. Brokmeier, Physica B: Condensed Matter **385-386**, Part 1, 623-625 (2006).

[5] H.-G. Brokmeier, In: Advanced Materials 2005 eds: M. Farooque, S.A. Rizvi, J.A. Mirza KRL Rawalpindi Pakistan 292-301 (2007).

[6] H.-G. Brokmeier, U. Zink, T. Reinert, W. Murach, J. Appl. Crys. **29**, 501 (1996).

[7] H.-G. Brokmeier, W. Ye, S.B. Yi, B. Schwebke, J. Homeyer, HASYLB Annual Report 2003, 305 (2003).

[8] J.F.H. Clusters, Philips Techn. Rundschau **7**, 13-20 (1942).

[9] G. Wassermann, J. Grewen, Texturen Metallischer Werkstoffe, Springer Verlag Berlin 1962.

[10] H.R. Wenk, Eine photographische Röntgengefügeanalyse, Schweiz. Min. Petr. Mitt. **45**, 518-550 (1965).

[11] H.J. Bunge, Adv. X-ray Analysis **47**, 420-430 (2004).

[12] S. Ahzi, A. Molinari, G.R. Canova, Acta Metall. **35**, 2983-2994 (1987).

[13] R.A. Lebensohn, C.N. Tomé, Acta Metall. Mater. **41**, 2611-2624 (1993).

[14] S.-B. Yi, C.H.J. Davis, H.-G. Brokmeier, R.E. Bolmaro, K.U. Kainer, J. Homeyer, Acta Mat. **54**, 549-562 (2006).

[15] S.B. Yi, H.-G. Brokmeier, R. Bolmaro, K.U. Kainer, J. Homeyer, Mater. Sci. Forum **495-497**, 1585-1590 (2005).

[16] S.-B. Yi, PhD-Thesis Clausthal University of Technology (2005).

[17] C.H.J. Davies, S.B. Yi, J. Bohlen, K.U. Kainer, H.-G. Brokmeier, J. Homeyer, Mater. Sci. Forum **495-497**, 1633-1638 (2005).

[18] H.-G. Brokmeier, S.B. Yi, B. Schwebke, J. Homeyer, Z. Kristallographie, (2007) in press.

Received: 3 December 2007.